REDOX REPORT
2025, VOL. 30, NO. 1, 2503130
https://doi.org/10.1080/13510002.2025.2503130

Taylor & Francis
Taylor & Francis Group

Kaempferol protects against doxorubicin-induced myocardial damage by inhibiting mitochondrial ROS-dependent ferroptosis

Lin Zhang[a], Xiaorui Liu[a], Juan Wang[a], Zimu Li[a], Siqi Wang[a], Wen Yang[a], Yang Hai[a,d] and Dongling Liu[a,b,c]

[a]School of Pharmacy, Gansu University of Chinese Medicine, Lanzhou, People's Republic of China; [b]Gansu Pharmaceutical Industry Innovation Research Institute, Gansu University of Chinese Medicine, Lanzhou, People's Republic of China; [c]Northwest Collaborative Innovation Center for Traditional Chinese Medicine, Lanzhou, People's Republic of China; [d]Key Laboratory of Dunhuang Medicine, Ministry of Education, Lanzhou, People's Republic of China

ABSTRACT

Background: Doxorubicin (DOX), a widely used chemotherapeutic agent, is limited in clinical application due to its dose-dependent cardiotoxicity. Therefore, it is crucial to explore alternative therapeutic molecules or drugs for mitigating DOX-induced cardiomyopathy (DIC). In this study aimed to explore underlying mechanisms of the cardioprotective effects of Kaempferol (KP) against DIC.

Methods: H9c2 cell-based DIC model were established to explore the pharmacological mechanism. The levels of mitochondrial membrane potential, mitochondrial ROS, mitochondrial Fe^{2+} and lipid peroxidation were detected using JC-1, TMRE, Mito-SOX, Mito-Ferro Green and C11-BODIPY 581/591 probes. Furthermore, Western blot analysis measured the expression of key regulatory proteins, and NRF2-targeting siRNA was transfected into H9c2 cells. The nuclear translocation of NRF2 was assessed by immunofluorescence.

Results: Data revealed that KP mitigated DOX-induced mitochondrial damage and ferroptosis via reducing membrane potential, mitochondrial ROS/Fe^{2+}, and regulating lipid metabolism. Mechanistically, Western blot analysis revealed that KP inhibited DOX-induced ferroptosis by activating NRF2/SLC7A11/GPX4 axis. Moreover, KP promoted the accumulation and nuclear translocation of NRF2 protein.

Conclusion: These findings demonstrated that KP protected against DOX-induced myocardial damage by inhibiting mitochondrial ROS-dependent ferroptosis. This provides novel insights into KP as a promising drug candidate for cardioprotection.

KEYWORDS
KP; DOX; cardiotoxicity; cardiomyocytes; mitochondrial ROS; ferroptosis; oxidative stress; action mechanism

1. Introduction

DOX is a powerful chemotherapeutic agent widely used in treating various malignancies, including leukemia, lymphoma, breast cancer, lung cancer, and sarcoma [1]. Despite its impressive anti-tumor efficacy, DOX administration is significantly limited by its dose-dependent cardiotoxicity, which manifests as vascular injury and cardiac fibrosis [2, 3]. The primary determinants of the development of heart failure are the cumulative dose of DOX, with a sharp increase in the incidence of heart failure occurring at a cumulative dose of 550 mg/m^2 [4, 5]. Dexrazoxane is the only drug approved by the FDA for prophylaxis against DOX-induced cardiotoxicity, but it has been found to pose a potential risk of secondary tumors in cancer patients. Therefore, exploring new alternative therapeutic drugs to alleviate the cardiotoxicity and preserve the anticancer activity of DOX has been a recent trend.

The concept of ferroptosis, first identified in 2012 [6], represents a distinct form of regulated cell death characterized by iron-dependent activation of lipoxygenases, leading to cell death through excessive lipid peroxidation [7–9]. Emerging evidence has established ferroptosis as a key mechanism underlying DOX-induced cardiotoxicity [10]. Specifically, DOX promotes mitochondrial iron overload by the formation of DOX-Fe^{2+} complexes, which disrupts iron homeostasis and triggers lipid peroxidation on mitochondrial membranes. Fang et al further identified hemosiderosis as a central driver of DIC [11]. Nuclear factor erythroid 2-related factor 2 (NRF2), a master regulator of antioxidant defense, plays a pivotal role in counteracting ferroptosis. DOX suppresses NRF2 activity, leading to glutathione peroxidase 4 (GPX4) downregulation and impaired lipid peroxidation repair [10]. Mitochondria are the primary site of DOX-induced ferroptosis. Excess free iron accumulated in mitochondria and causes lipid peroxidation on their membranes [12]. Moreover, mitochondria-targeted antioxidant mitoTEMPO significantly rescued DOX cardiomyopathy, supporting oxidative damage of mitochondria as a major mechanism in ferroptosis-induced heart damage [13, 14]. Therefore, targeting ferroptosis could serve as a strategy for preventing cardiomyopathy.

Kaempferol (KP), a natural flavonoid compound widely distributed in plants [15], has garnered significant attention due to its remarkable antioxidant, immunomodulatory and anti-apoptotic properties. A diet containing KP may be beneficial for those who are at risk of myocardial injury. Previous research indicated that KP can protect the vascular

CONTACT Dongling Liu dongling83@163.com School of Pharmacy, Gansu University of Chinese Medicine, Lanzhou, Gansu 730000, People's Republic of China; Gansu Pharmaceutical Industry Innovation Research Institute, Gansu University of Chinese Medicine, Lanzhou, Gansu 730000, People's Republic of China; Northwest Collaborative Innovation Center for Traditional Chinese Medicine, Lanzhou 730000, People's Republic of China

endothelium against DOX-induced damage by inhibiting oxidative stress and improving mitochondrial function [16]. It effectively protects cardiomyocytes against A/R injury through a mitochondrial pathway mediated by SIRT1 [17]. Moreover, KP inhibits cisplatin-induced cardiotoxicity [13]. KP provides protection from OGD/R-induced ferroptosis partly by activating NRF2/SLC7A11/GPX4 signaling pathway [18]. Therefore, it is preliminarily speculated that the role of KP may be related to the mitochondrial-mediated ferroptosis effect. The current study explored the possible mechanisms of KP on DIC through induction of cardiotoxicity.

In the study, we established Erastin-induced ferroptosis model in H9c2 cells, and demonstrated that KP can inhibit ferroptosis. Further, by employing DOX to establish a myocardial injury model, we confirmed that KP can inhibit DOX-induced ferroptosis by reducing mitochondrial ROS and lipid peroxidation. KP may inhibit DOX-induced mitochondrial reactive oxygen species (ROS)-dependent ferroptosis via the NRF2/SLC7A11/GPX4 pathway. These findings provided novel insights into the cardioprotective effects of KP against DOX-induced cardiotoxicity.

2. Material and methods

2.1. Cell culture and processing

H9c2 cells (embryonic rat cardiomyocyte cell line) and AC16 cells (adult human cardiomyocyte cell line) were purchased from Cell Bank of the Chinese Academy of Sciences, Shanghai, China, and the cells were cultured in high-sugar DMEM medium (Thermo Fisher Scientific, Waltham, Mass. Waltham, MA,8123565) supplemented with 10% (v/v) fetal bovine serum (TianHang Biotechnology, 200704, Zhejiang, China) and 1% (v/v) antibiotics (10,000 U/ml penicillin and 10 mg/ml streptomycin, 20221231, solarbio, Beijing, China). H9c2 cells were incubated at 37°C in a mixture of 95% atmospheric air and 5% CO_2, and the culture medium was replaced every two days. Cells were treated with 2 μM DOX alone or in combination with 1 μM Ferrostatin-1 (Fer-1), 32 μM Erastin, 8 μM mitoTEMPO, 2.5 μM TBHQ, 100 U/mL PEG-SOD or KP (40, 80, 160 μM). Subsequently, H9c2 cell survival was detected using MTT colorimetric assay, and changes in SOD (A001-3-1, Nanjing Jiancheng), LDH (A020-2-1, Nanjing Jiancheng), GSH (A006-2-1, Nanjing Jiancheng), and GSH-px (A005-1-2, Nanjing Jiancheng) content in H9c2 cell supernatants or cells were determined to assess the extent of cardiomyocyte injury.

2.2. Reactive oxygen detection

Cellular ROS levels were measured according to the manufacturer's instructions (S0033S, Biyun Tian, China). Cells at specific interventions were incubated with DCFH-DA for 20 min. Cells were washed in PBS prior to analysis using a flow cytometer (BD Biosciences). Mean fluorescence intensity was analyzed using FlowJo (version 10.6.2; FlowJo LLC).

2.3. JC-1 detect mitochondrial membrane potential

Membrane potential of cells for specific interventions was determined using the Mitochondrial Membrane Potential Assay Kit (M8650, Solarbio, Beijing). H9c2 cells were inoculated in six-well plates and stained with JC-1 in working solution for 20 min prior to flow cytometry analysis (BD Biosciences), following the instructions.

2.4. TMRE detect mitochondrial membrane potential

H9c2 cells were cultured in six-well plates, cells were incubated with 1 mM Hoechst 33258 (C0021, Solarbio, Beijing) and 100nM TMRE co-staining for 30 min at 37°C washed three times with PBS to remove the fluorescent probe and were then analyzed using a fluorescence microscope (Ts2-FL, Nikon, China)

2.5. Detection of mitochondrial ROS

H9c2 cells were cultured in six-well plates, the cells were incubated with 150 nM MitoTracker green (GC26229, GLPBIO) for 30 min with PBS for three times and then stained with 1 μg/mL Hoechst for 25 min at 37°C. And cells were incubated with 5 μM MitoSOX Red (GC68230, GLPBIO) in the dark for 10 min at 37°C. Afterward, cells were washed three times with PBS to remove the dye. Confocal fluorescence microscope (Ts2-FL, Nikon, China) was used for observation and photo analysis.

2.6. Detection of lipid peroxidation

The H9c2 cells were incubated with C11-BODIPY (S0043S, Biyun Tian, China) at 37°C for 30 min. After incubation, cells were washed with PBS for three times. Fluorescence was measured using a fluorescence microscope (Ts2-FL, Nikon, China), which also was utilized for visualization.

2.7. Cellular mitochondrial Fe^{2+} assay

The H9c2 cells were incubated with 0.1 mol/L Mito-Ferro Green (M489, Dojindo, Kumamoto, Japan) and MitoBright LT Deep Red (MT11, Dojindo, Kumamoto, Japan) at 37°C for 30 min. The cells were then washed twice with PBS and then stained with 1 μg/mL Hoechst 33,258 for 25 min at 37°C. Afterward, cells were washed with PBS for three times to remove the dye. Fluorescence was measured using a fluorescence microscope (Ts2-FL, Nikon, China), which also was utilized for visualization.

2.8. Transmission electron microscope assay

Cells were fixed for electron microscopy. Wash twice with PBS and ethanol, then dehydrate with 100% acetone for about 10 min. Mix the acetone with the embedding medium at a 1:1 (v/v) ratio and immerse at room temperature for 2 h. Embed using epoxy resin overnight at 35°C. Cure in an oven at 45°C for 24 h. Then, section and stain with uranyl acetate and lead citrate, incubating at 66°C overnight, and mitochondrial morphology was observed using transmission electron microscopy.

2.9. siRNA transfection

H9c2 cells were transfected with small interfering RNA (siRNA) designed to target NRF2, as well as control siRNAs (GenePharma), utilizing the siRNA-mate plus transfection reagent (GenePharma), in accordance with the manufacturer's guidelines. Following a period of 72 h post-transfection, the cells were collected and subjected to western blot analysis to

ascertain the efficacy of NRF2 knockdown. Cells were divided into: (i) Ctrl; (ii) DOX; (iii) DOX + siRNA; (iv) DOX + KP; (v) DOX + KP + NRF2 siRNA. Subsequent to these treatment regimens, the cells were harvested for subsequent analyses.

2.10. Immunofluorescence

H9c2 cells were grown on a laser confocal dish, and then fixed with 4% paraformaldehyde for 15 min, followed by permeabilization for 20 min and blocked with normal goat serum for 1 h. Later, cells were incubated with NRF2 antibody overnight at 4°C, followed by incubation with secondary antibody for 1 h. After being washed three times with PBS, cells were counterstained with Hoechst 33,258 (1 μg/ml) for 5 min. Images were then taken with a confocal microscopy.

2.11. Western blotting

H9c2 cells of specific interventions were collected, lysed by adding RIPA lysate, total protein was extracted, SDS-PAGE electrophoresis was performed, the membrane was flowed for 90 min at 200 mA constant flow, blocked with 5% (w/v) skimmed milk for 2 h, and washed with TBST for 30 min. All antibodies were diluted according to the manufacturer's instructions. Subsequently, the membrane was incubated with the corresponding primary and secondary antibodies. Protein signals were detected using enhanced chemiluminescence (ECL) reagents and quantified using ImageJ software.

2.12. Reagents and antibodies

KP (CFN92386, purity ≥ 98%) was procured from ChemFaces Biochemical Co., Ltd. (China). DOX (1015P023) was obtained from Solarbio. Erastin (HY-15763), Fer-1 (HY-100579) and TBHQ (HY-100489) were purchased from MedChemexpress Ltd (New Jersey, USA). mitoTEMPO (A20224, Adoop, USA). PEG-SOD (S9549, Merck). Primary antibodies included Primary antibodies included SLC7A11 (#D2M7A, Thermo Fisher Scientific), GPX4 (#YN3047, Immunoway), NRF2 (#YT3189, Immunoway), ACSL4(#abs106075, Absin), FTL (#TD6604s, Abmart), FTH1 (#D1D4, Cell signaling), and GAPDH (#abs830030ss, Absin).

2.13. Statistical analyses

All experimental data obtained were expressed as mean ± SEM. Statistical analyses between groups were compared were performed using Graphpad Prism software version 8.0. Multiple groups of samples were compared using one-way ANOVA, if they obeyed normal distribution and homogeneity of variance. A *t*-test was used to compare differences between groups. Further, $p < 0.05$ or $p < 0.01$ were considered statistically significant.

3. Results

3.1. KP alleviated DOX-induced myocardial damage

To investigate the effect of KP on cardiac function in cases of DOX-induced myocardial damage, experiments were performed using MTT assay to explore the effect of different concentrations of KP on DOX-induced cardiotoxicity in H9c2 cells. Results showed that KP at 40, 80 and 160 μM were the more effective concentrations for attenuating the decrease in viability of DOX-treated H9c2 cells (Figure 1(A, B)). Subsequent experiments were conducted using these concentrations. Myocardial injury and oxidative stress were further assessed by measuring lactate dehydrogenase (LDH), superoxide dismutase (SOD), glutathione (GSH), and glutathione peroxidase (GSH-Px) activities. Compared with the control group, the DOX model group exhibited significantly elevated LDH activity and reduced SOD, GSH, and GSH-Px activities. KP treatment decreased LDH release and restored SOD, GSH, and GSH-Px activities to near-normal levels (Figure 1(C–F)). These results demonstrated that KP mitigated DOX-induced cardiomyocyte damage by counteracting oxidative stress.

3.2. KP protected DOX-induced myocardial damage by counteracting ferroptosis

To elucidate whether ferroptosis contributes to DOX cardiotoxicity, we treated H9c2 cells with the ferroptosis inhibitor Fer-1 before DOX treatment. Then, we measured the levels of Fe^{2+}, measured ROS levels using DCFH-DA, and detected the levels of SLC7A11, GPX4, and ACSL4 after treatment of DOX in combination with Fer-1. Fer-1 significantly suppressed DOX-induced intracellular Fe^{2+} accumulation and ROS overproduction (Figure 2(A–D)). Western blot analysis revealed that DOX markedly upregulated the lipid peroxidation marker ACSL4 while downregulating SLC7A11 and GPX4 expression, Fer-1 reversed DOX-induced reduction of GPX4 and SLC7A11 protein and increase ACSL4 in cardiomyocytes (Figure 2(E–H)). Notably, KP (160 μM) mirrored the effects of Fer-1. These results proved that DOX-induced myocardial damage via ferroptosis, and KP exerted cardioprotection by targeting key ferroptosis pathways.

3.3. KP rescued disruption of iron homeostasis and lipid peroxidation induced by erastin

To validate KP anti-ferroptotic effects, we employed Erastin, a canonical ferroptosis inducer that binds to the cystine/glutamate antiporter SLC7A11, blocking cystine uptake and depleting glutathione (GSH) biosynthesis, thereby downregulating GPX4 and amplifying lipid peroxidation (Figure 3(D–F)). Flow cytometry revealed that KP significantly reduced Erastin-induced intracellular ROS levels (Figure 3(A)). MitoSOX staining further demonstrated that KP suppressed red fluorescence intensity triggered by Erastin-induced mitochondrial ROS burst (Figure 3(B)). Lipid peroxidation, a hallmark of ferroptosis, was assessed using the C11-BODIPY 581/591 probe. Erastin treatment markedly increased green fluorescence, while Fer-1 and KP treatments suggested that KP significantly inhibited Erastin-induced mitochondrial lipid peroxidation, thereby suppressing ferroptosis (Figure 3(C)). Furthermore, KP restored GSH and GSH-Px activities (Figure 3(D–F)), demonstrating strong antioxidant capacity. These results showed that KP exerted similar anti-ferroptotic effects by targeting lipid peroxidation and iron metabolism.

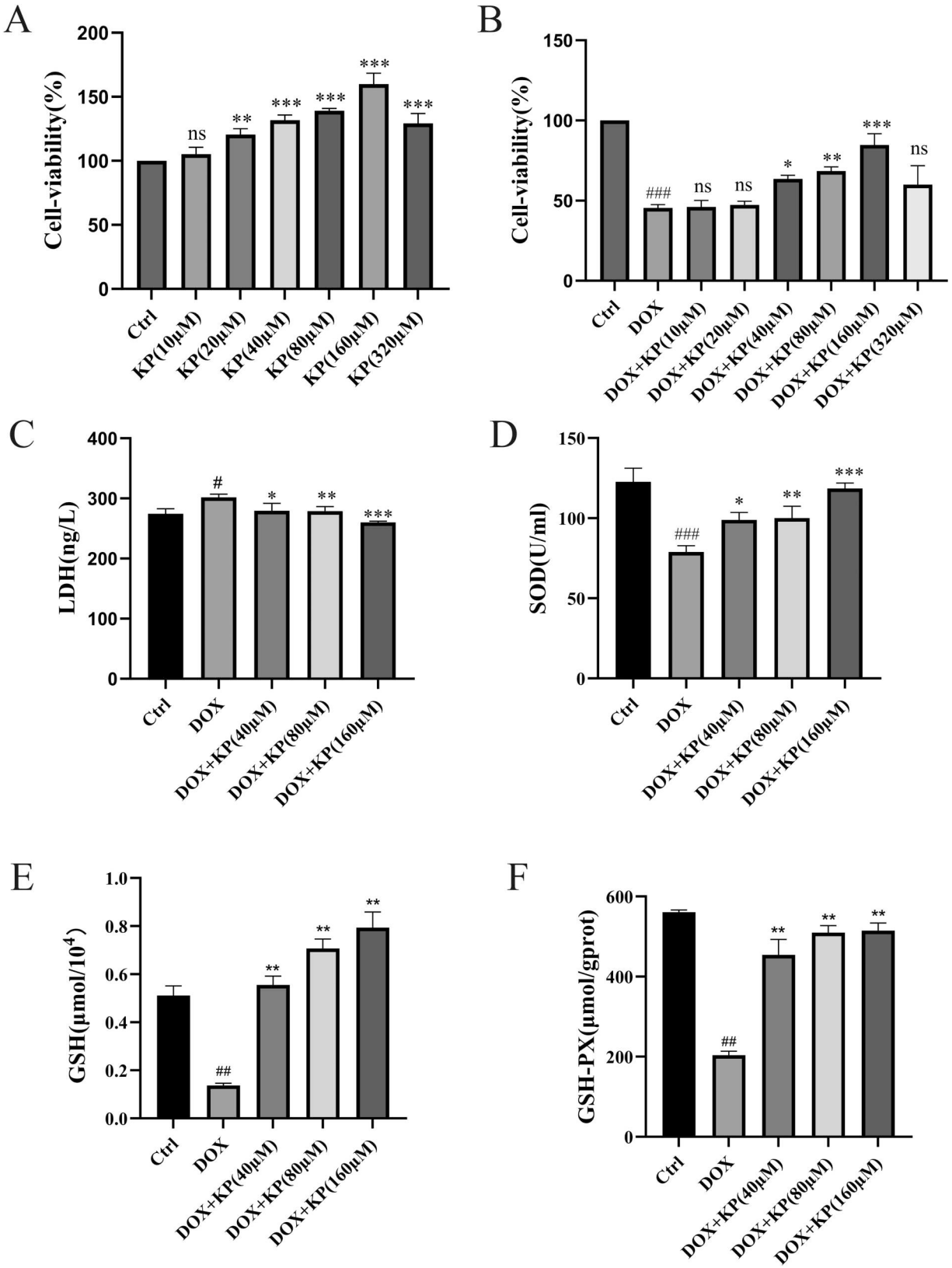

Figure 1. KP alleviated DOX-induced myocardial damage (A) Cell viability assay of H9c2 cardiomyocytes when treated with 0, 10, 20, 40, 80, 160, 320 μM of KP for 24-h, $n = 3$. (B) H9c2 cells were cultured with 2 μM DOX in combination with KP at various concentrations (0, 10, 20, 40, 80, 160, 320 μM) for 24-h. Cell viability was measured by MTT method, $n = 3$. (C–F) Effect of KP administration on DOX-induced myocardial injury and oxidative stress damage markers LDH, SOD, GSH, and GSH-px activity in H9c2 cardiomyocytes, $n = 3$. Data were expressed as mean ± SEM of three independent replicates; $^{\#}P < 0.05$, $^{\#\#}P < 0.01$, $^{\#\#\#}P < 0.001$ vs. control group; $^{*}P < 0.05$, $^{**}P < 0.01$, $^{***}P < 0.001$ vs. DOX group.

3.4. KP attenuated mitochondrial damage in erastin-induced ferroptosis

We further evaluated the protective effect of KP on Erastin-induced mitochondrial damage in H9c2 cardiomyocytes. H9c2 cells were detected with the fluorescent probe JC-1 and fluorochrome TMRE to observe changes in the mitochondrial membrane potential of H9c2 cells (Figure 4(A,B)). We observed that Erastin caused a decrease in cellular mitochondrial membrane potential in H9c2 myocardial damage, and KP attenuated the Erastin-induced decrease in mitochondrial

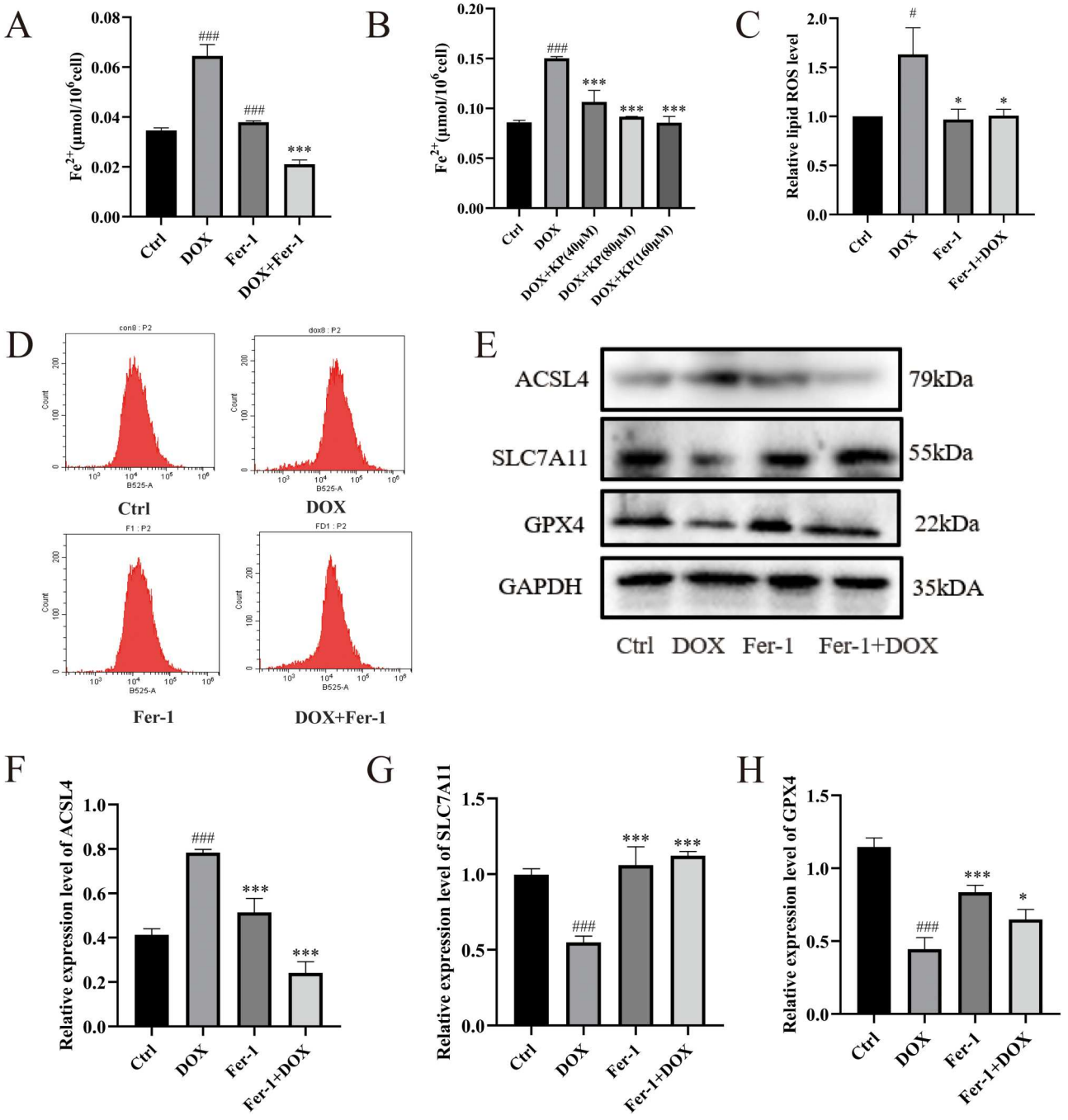

Figure 2. KP protected DOX-induced myocardial damage by counteracting ferroptosis. (A,B) The level of Fe^{2+} in H9c2 cardiomyocytes after 24-h treatment of DOX (2μM) in combination with Fer-1 (1μM) or KP after 24-h treatment of DOX in combination with Fer-1, $n = 3$. (C,D) H9c2 cells were analyzed by flow cytometry with DCFH-DA after 24-h treatment of DOX (2μM) in combination with Fer-1, $n = 2$. (E–H) Representative protein blotting bands of GPX4, SLC7A11 and ACSL4 in H9c2 cells with GAPDH as internal reference after 24-h treatment of DOX in combination with Fer-1, $n = 3$. Data were expressed as mean ± SEM; $^{\#}P < 0.05$, $^{\#\#\#}P < 0.001$ vs. control group; $^{*}P < 0.05$, $^{***}P < 0.001$ vs. DOX group.

membrane potential. Moreover, it was noted that treatments with KP inhibited Erastin-induced over-accumulation in the levels of mitochondrial Fe^{2+} (Figure 4(C)). In conclusion, these findings indicated that KP played a vital role in mitochondrial regulation of the anti-ferroptosis activity.

3.5. KP mitigated DOX-induced cardiomyocyte ferroptosis via suppressing mitochondrial ROS-dependent lipid peroxidation

Our findings also demonstrated that DOX-induced mitochondrial damage and excessive ROS production led to cardiomyocyte ferroptosis. Staining with DCFH-DA (a general ROS probe) revealed that DOX significantly increased ROS levels in H9c2 cells, while KP suppressed DOX-induced ROS (Figure 5(A,B)). MitoSOX was used to detect mitochondrial ROS generation induced by DOX. (Figure 5(C)), The C11-BODIPY 581/591 fluorescence staining showed KP reduced green fluorescence intensity triggered by DOX (Figure 5(D)). Consistent with the above results, both Fer-1 and KP inhibited the lipid peroxidation induced by DOX. These results showed that KP lowered DOX-induced lipid peroxidation and thereby mitigating ferroptosis.

3.6. KP reversed DOX-induced mitochondrial damage and ferroptosis through Fe^{2+} homeostasis regulation.

Previous studies have reported that DOX induces mitochondrial Fe^{2+} leading to mitochondrial lipid peroxidation and thus promoting ferroptosis [19]. In a highly consistent

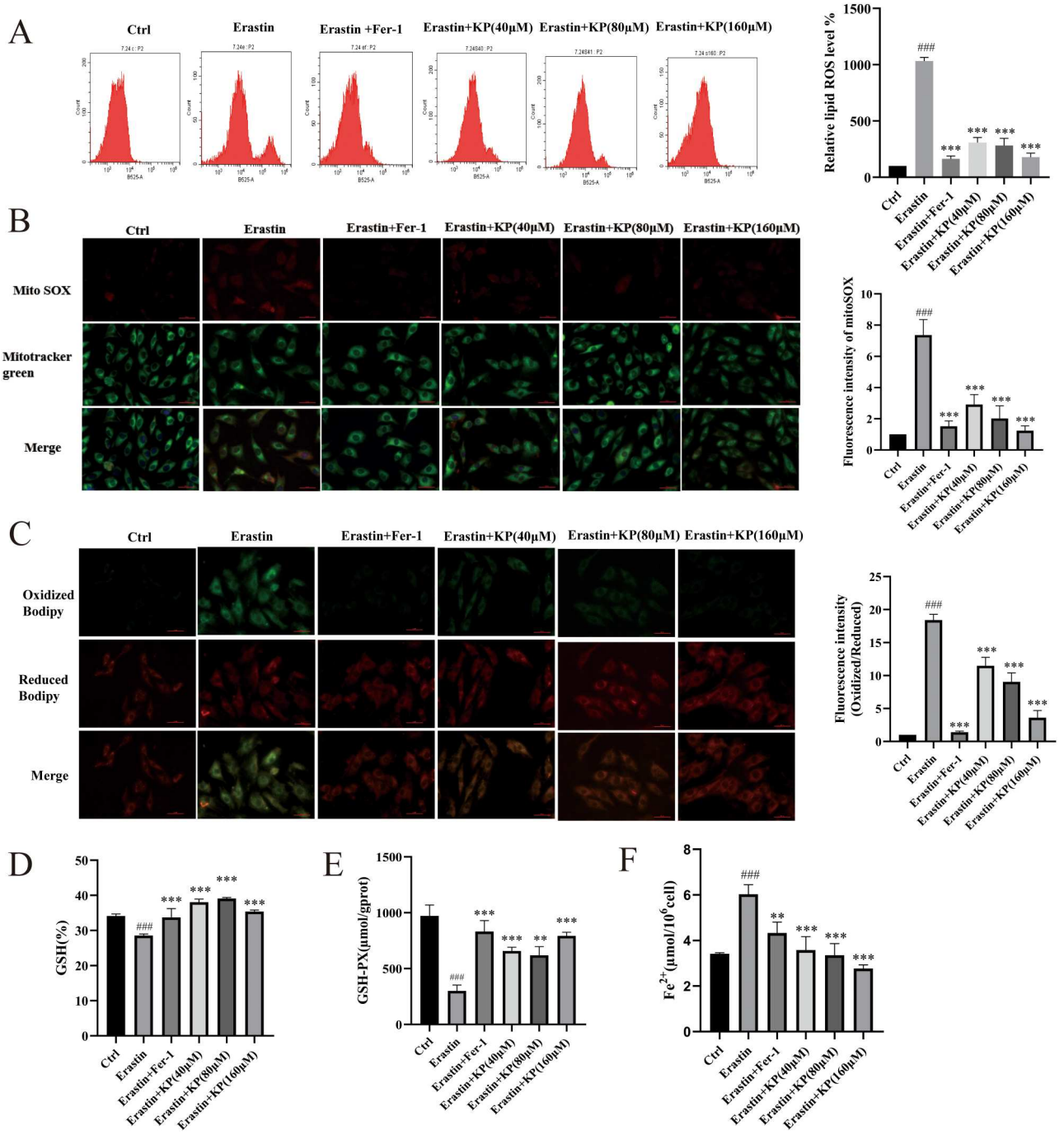

Figure 3. KP rescued disruption of iron homeostasis and lipid peroxidation induced by Erastin. (A) H9c2 cells were analyzed by flow cytometry with DCFH-DA after 24-h treatment of Erastin (32μM) in combination with Fer-1 or KP, $n = 2$. (B) Images of MitoSOX stained H9c2 cells, and the histogram showed MitoSOX fluorescence. Scale bar=50 μm, $n = 3$. (C) Images of C11-BODIPY 581/591 stained H9c2 cells. Histogram presented fluorescence intensity of oxidized BODIPY (Oxidized/Reduced). Histogram presented fluorescence intensity of oxidized BODIPY. Scale bar=50 μm, $n = 3$. (D–F) Effect of KP and Fer-1 administration on Erastin-induced oxidative stress damage markers GSH, GSH-px activity and the level of Fe^{2+}, $n = 3$. Data were expressed as mean ± SEM; $^{###}P$ <0.001 vs. control group; $^{**}P < 0.01$, $^{***}P < 0.001$ vs. DOX group.

manner, our study's results converged on the same conclusion, further validating the established mechanism. As shown in Figure 6(A), DOX caused distinct mitochondrial morphological changes in H9c2 cells, where the cristae of mitochondria were disordered and disappear, mitochondria smaller, and inner membrane folding was disrupted. In JC-1 assays, which were employed to evaluate mitochondrial membrane potential (MMP), treatment with carbonyl cyanide m-chlorophenylhydrazone (CCCP) functioned as a potent positive control. This treatment successfully triggered MMP dissipation, thereby confirming both the functionality of the probe and the reliability of the experimental design. Furthermore, JC-1 and TMRE staining demonstrated that in DOX-treated H9c2 cells, MMP levels increased (Figure 6(B,C)), and Mito-Ferro Green indicated an increase in mitochondrial Fe^{2+} levels (Figure 6(D)). In this study, accompanied by a decrease in mitochondrial membrane potential. KP treatment partially rescued mitochondrial defects and reversed the damage to mitochondria in DOX-induced H9c2 cells, subsequently reducing mitochondrial membrane potential and mitochondrial Fe^{2+} levels. These results suggested that KP attenuated DOX-induced mitochondrial damage to cardiomyocytes by inducing ferroptosis.

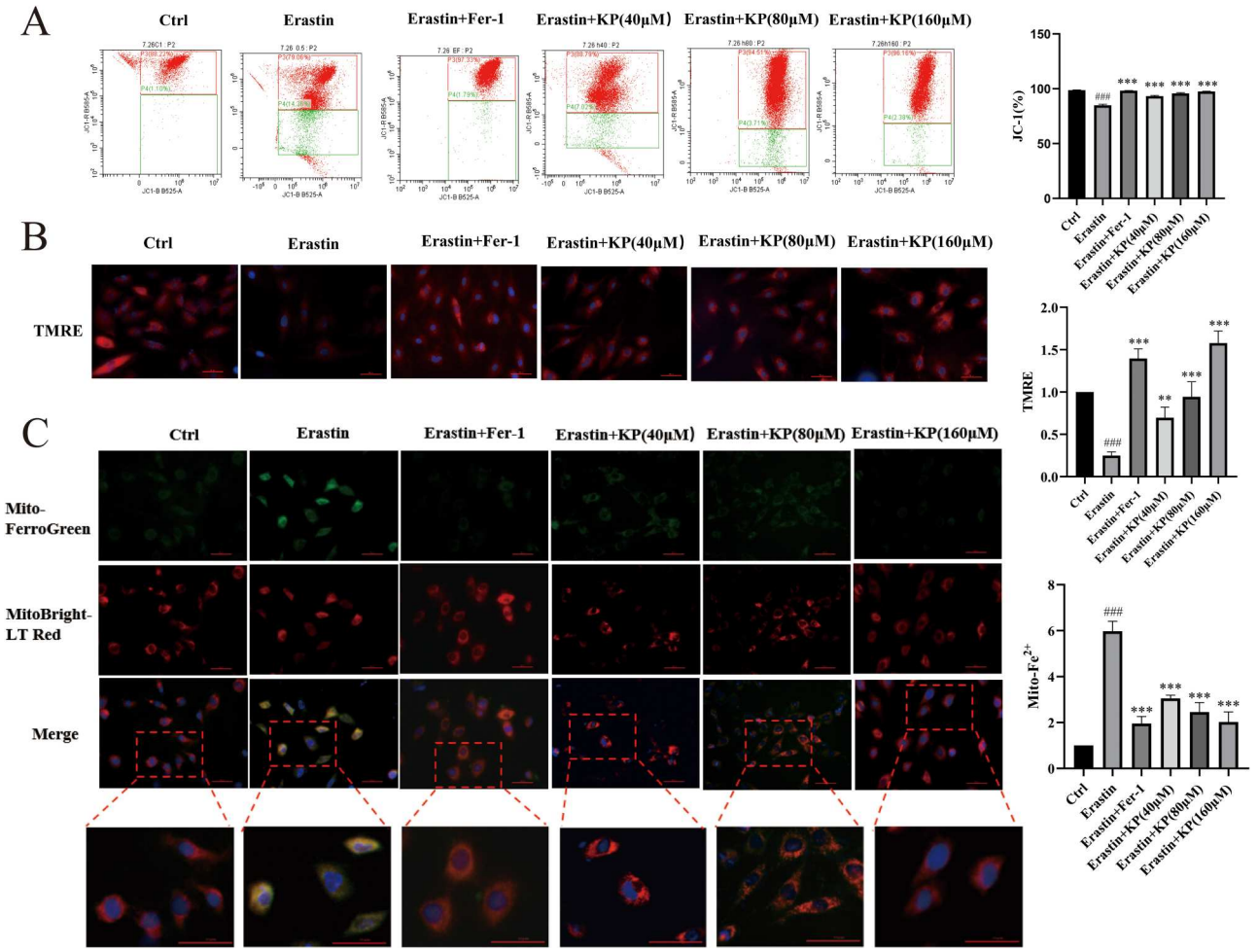

Figure 4. KP attenuated mitochondrial damage in Erastin-induced ferroptosis. (A) H9c2 cells were stained with JC-1 and analyzed by flow cytometry after 24-h treatment of Erastin in combination with Fer-1 or KP. Two independent experiments were performed, $n = 2$. (B) Images of TMRE stained H9c2 cells, and the histogram showed TMRE fluorescence. Scale bar=50 μm, $n = 3$. (C) Images of Mito-Ferro Green staining stained H9c2 cells, and the histogram showed Mito-Ferro Green fluorescence, detecting mitochondrial Fe^{2+} level. Scale bar=50 μm, $n = 3$. Data were expressed as mean ± SEM; $^{###}P$ <0.001 vs. control group; $^{**}P < 0.01$, $^{***}P <$ 0.001 vs. DOX group.

3.7. KP restored mitochondrial function and attenuated DOX-induced ferroptosis via ROS scavenging and Fe^{2+} homeostasis regulation

To validate the role of mitochondrial ROS in DOX-induced ferroptosis, we treated cells with mitoTEMPO (a mitochondria-targeted superoxide scavenger with dual roles as a SOD mimetic and radical scavenger) and PEG-SOD (a systemic antioxidant selectively neutralizing extracellular superoxide radicals). To evaluate mitochondrial dysfunction, ROS levels, and lipid peroxidation in DOX-treated H9c2 cells, we measured TMRE fluorescence, MitoSOX signal, and C11-BODIPY oxidation. In cellular ROS assays, the positive control Rosup significantly increased ROS levels, validating detection sensitivity. Both mitoTEMPO and KP significantly alleviated DOX-induced mitochondrial dysfunction (Figure 7(A)), suppressed mitochondrial ROS (Figure 7(B)), and attenuated lipid peroxidation (Figure 7(C)). While mitoTEMPO primarily targeted mitochondrial ROS, PEG-SOD reduced extracellular oxidative stress. KP mirrored mitochondrial protection, attenuating DOX-induced ferroptosis by reducing mitochondrial Fe^{2+} (Figure 6(D)) and ROS accumulation (Figure 7(C)). Importantly, the application of mitoTEMPO and PEG-SOD further suppressed total ROS levels (Figure 7(D)) and restored SOD activity (Figure 7(E)). However, KP efficacy in targeting mitochondrial ROS (similar to mitoTEMPO) highlights its potential as a mitochondria-specific ferroptosis inhibitor. These data collectively demonstrated that DOX triggers ferroptosis via mitochondrial ROS overproduction, and both KP and mitoTEMPO counteracted this pathway through localized antioxidant mechanisms. In cellular ROS assays, the positive control Rosup significantly increased ROS levels, validating detection sensitivity.

3.8. KP attenuated DOX cardiotoxicity by activating NRF2/SLC7A11/GPX4 pathway to suppress mitochondrial ROS-driven ferroptosis

This study demonstrated that DOX and Erastin significantly downregulated the expression of NRF2, SLC7A11, GPX4, FTL, and FTH1 while upregulating the lipid peroxidation promoter ACSL4 in H9c2 cardiomyocytes. KP dose-dependently restored NRF2 expression and activated its downstream targets SLC7A11 and GPX4, concurrently enhancing iron storage through FTL/FTH1 and suppressing lipid peroxidation via ACSL4 reduction (Figure 8(A,B)). Complementary experiments validated NRF2 transcriptional role: The NRF2 activator TBHQ mimicked KP effects by upregulating SLC7A11/GPX4 (Figure 9(A)) and rescuing mitochondrial membrane potential (Figure 9(I)), whereas NRF2 siRNA knockdown abolished KP protection (Figure 9(B)). Immunofluorescence confirmed KP-

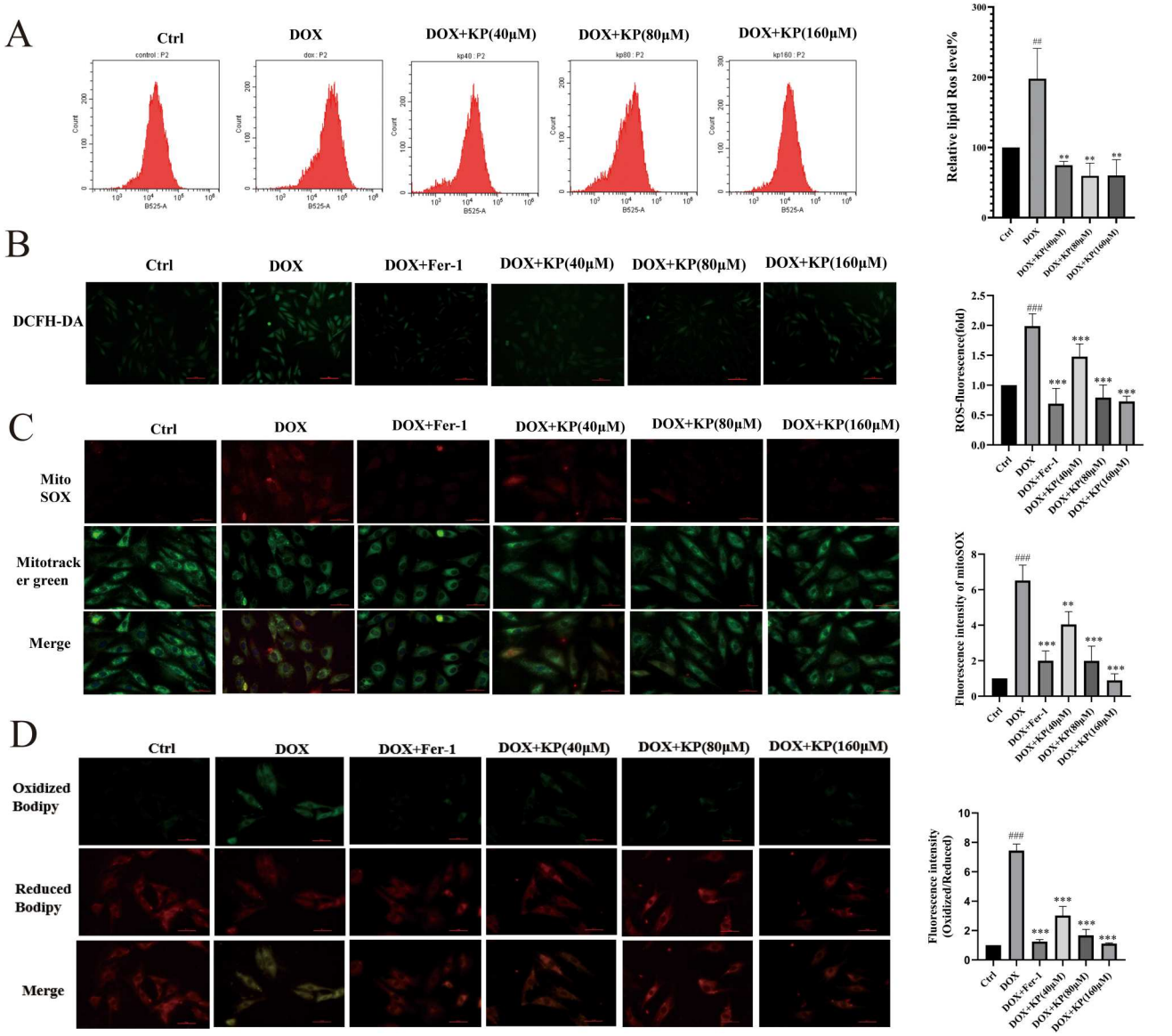

Figure 5. KP mitigated DOX-induced cardiomyocyte ferroptosis via suppressing mitochondrial ROS-dependent lipid peroxidation. (A,B) Images and level of DCFH-DA. and the histogram showed DCFH-DA fluorescence. Scale bar=100μm, $n = 2$. (C) Images of MitoSOX stained H9c2 cells, and the histogram showed MitoSOX fluorescence. Scale bar=50 μm, $n = 3$. (D) Images of C11-BODIPY 581/591 stained H9c2 cells. Histogram presented fluorescence intensity of oxidized BODIPY (Oxidized/Reduced) Scale bar=50 μm, $n = 3$. Data were expressed as mean ± SEM of three independent replicates; $^{\#\#}P < 0.01$, $^{\#\#\#}P<0.001$ vs. control group; $^{**}P < 0.01$, $^{***}P < 0.001$ vs. DOX group.

induced NRF2 nuclear translocation in DOX-treated cells (Figure 9(J)), indicative of transcriptional activation. Mitochondrial uncoupler CCCP exacerbated DOX-induced mitochondrial membrane potential loss, while KP and TBHQ restored mitochondrial membrane potential (Figure 9(I)). Collectively, KP alleviates DOX cardiotoxicity by activating NRF2 nuclear translocation, which transcriptionally upregulates SLC7A11 and GPX4 to suppress mitochondrial ROS-driven ferroptosis, highlighting the NRF2/SLC7A11/GPX4 axis as a pivotal mechanism for oxidative stress and iron homeostasis regulation.

3.9. KP protected human AC16 cardiomyocytes from DOX-induced ferroptosis via the NRF2/SLC7A11/GPX4 pathway

To validate KP protective effects against DOX-induced ferroptosis and enhance clinical relevance, we conducted complementary experiments in the human ventricular cardiomyocyte line AC16. MTT assays demonstrated that 40, 80, and 160 μM KP significantly restored viability in DOX-treated AC16 cells (Figure 10(A,B)). Western blot analysis revealed that DOX markedly downregulated NRF2, SLC7A11, and GPX4 expression in AC16 cells. Notably, KP intervention restored NRF2 and its downstream targets SLC7A11/GPX4 to near-control levels (Figure 10(C)), confirming the conservation of KP anti-ferroptosis mechanism via the NRF2/SLC7A11/GPX4 axis in human cardiomyocytes.

4. Discussion

DOX is a highly effective anti-tumor chemotherapeutic agent used in clinical practice for the treatment of a variety of cancers and solid tumors. A large body of evidence confirms that DOX induces cardiomyopathy [20]. Most cardiotoxicity after anthracycline-containing therapy occurs within the first year and is associated with anthracycline dose and LVEF at the end of treatment. Early detection and prompt therapy of cardiotoxicity appear crucial for substantial

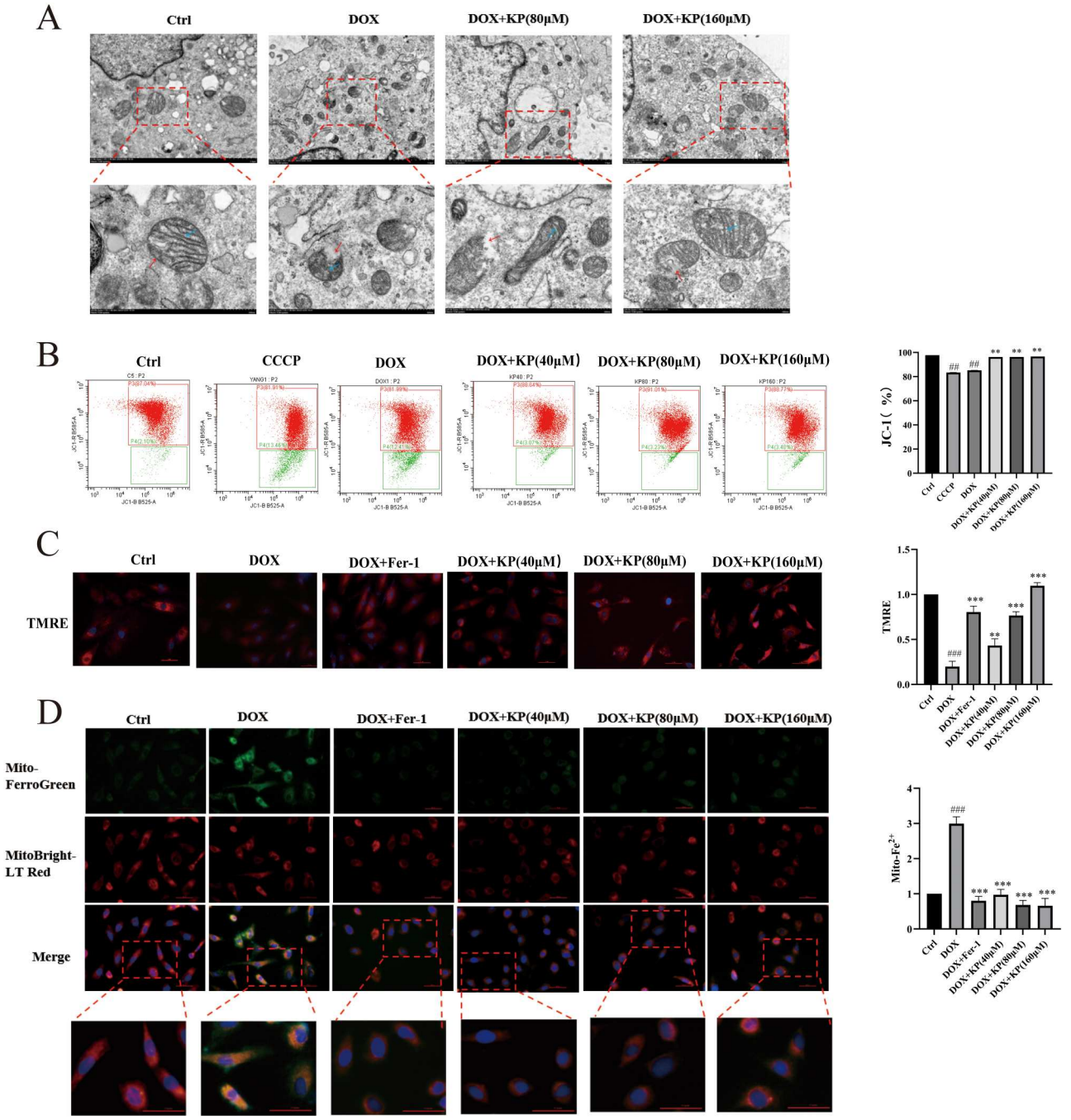

Figure 6. KP reversed DOX-induced mitochondrial damage and ferroptosis through Fe^{2+} homeostasis regulation. (A) Transmission electron microscope images of H9c2 cells. Enlarged inserts at the down side of each image showed typical morphology of mitochondria. Each pair of images had a scale indicated in the lower right corner of each image, while the lower left corner showed the magnification. The lower image was an enlarged version of the area within the yellow box. The red arrows represented the mitochondrial membrane, and the blue arrows indicated the mitochondrial cristae, $n = 3$. (B) H9c2 cells were stained with JC-1 and analyzed by flow cytometry. Two independent experiments were performed, $n = 2$. (C) Images of TMRE stained H9c2 cells, and the histogram showed TMRE fluorescence Scale bar=50 μm, $n = 3$. (D) Images of Mito-Ferro Green staining stained H9c2 cells, and the histogram showed Mito-Ferro Green fluorescence, detecting mitochondrial Fe^{2+} level. Scale bar=50 μm, $n = 3$.Data were expressed as mean ± SEM of three independent replicates; $^{\#\#}P < 0.01$, $^{\#\#\#}P < 0.001$ vs. control group; $^{**}P < 0.01$, $^{***}P < 0.001$vs. DOX group.

recovery of cardiac function [21]. The search for phytochemicals for the treatment of DIC has received increasing attention. In the current study, we demonstrated that KP exerts cardioprotective effects against DIC in H9c2 cells by targeting mitochondrial ROS-dependent ferroptosis. Specifically, KP significantly restored mitochondrial membrane potential, suppressed mitochondrial Fe^{2+} accumulation, and attenuated lipid peroxidation.

Recent studies have implicated ferroptosis in the pathogenesis of various cardiovascular diseases (CVDs), including DOX-induced cardiotoxicity [22, 23]. Our findings align with this paradigm: DOX treatment reduced mitochondrial membrane potential, increased ROS levels, and elevated lipid peroxidation markers, all hallmarks of ferroptosis. Fer-1, a canonical ferroptosis inhibitor, reversed these effects, confirming ferroptosis as a central mechanism in DOX cardiotoxicity [24–26]. Therefore, targeting ferroptosis is an effective cardioprotective strategy for cardiomyopathy prevention. CAO et al. [27] found that GSH is a sensitive indicator of ferroptosis. GPX4 acts as a guardian against lipid peroxidation and is regarded as an inhibitor of ferroptosis [12, 28]. The cystine/glutamate antiporter SLC7A11 (also known as xCT) functions to import cystine for glutathione biosynthesis and antioxidant defense [29]. The antioxidant

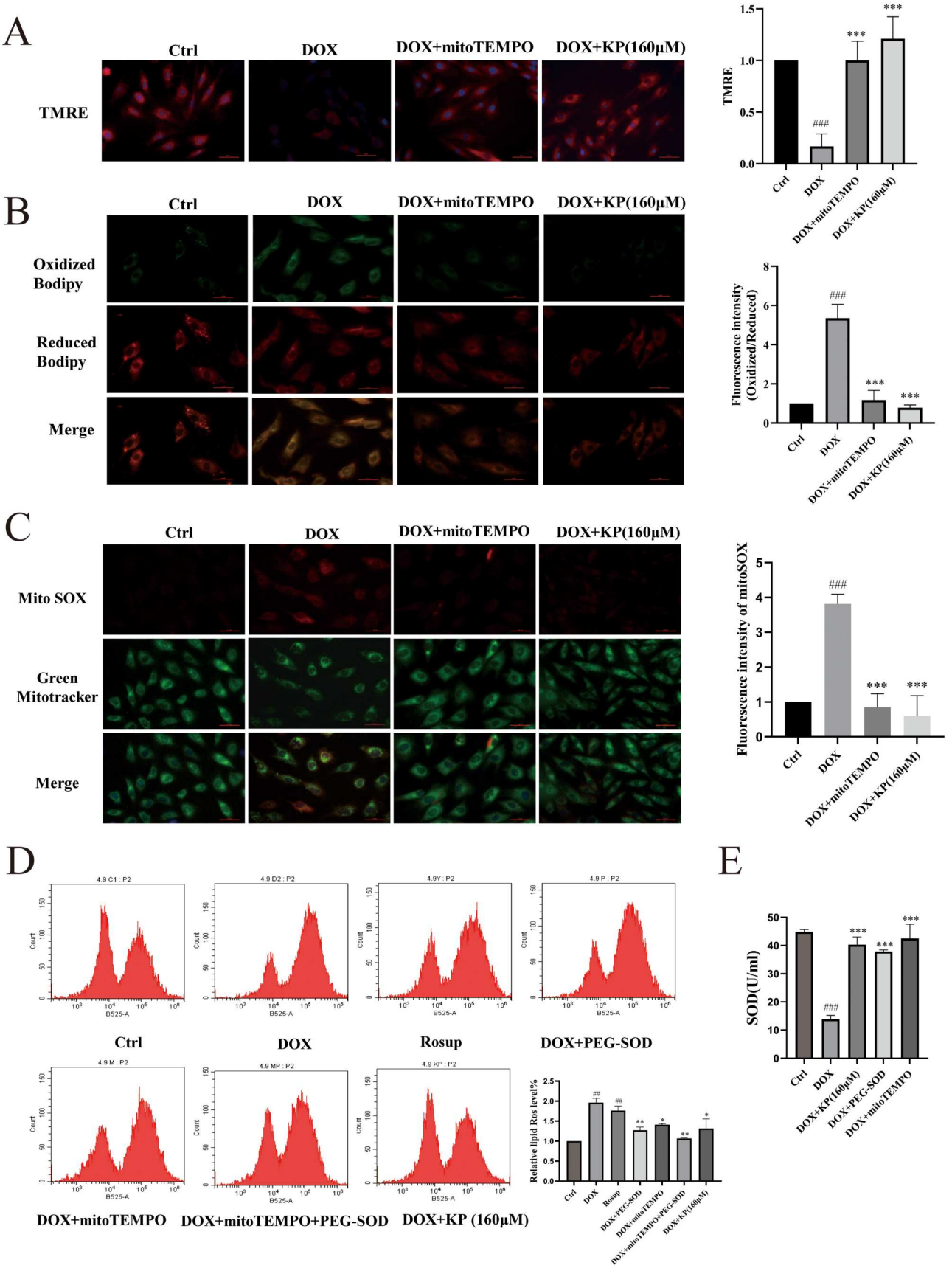

Figure 7. KP restored mitochondrial function and attenuated DOX-induced ferroptosis via ROS scavenging and Fe^{2+} homeostasis regulation. (A) Images of TMRE stained H9c2 cells after 24-h treatment of DOX in combination with or without mitoTEMPO (8μM) or KP, Scale bar=50 μm, $n = 3$. (B) Images of MitoSOX stained H9c2 cells, and the histogram showed MitoSOX fluorescence. Scale bar=50 μm, $n = 3$. (C) Images of C11-BODIPY 581/591 stained H9c2 cells. Histogram presented fluorescence intensity of oxidized BODIPY (Oxidized/Reduced) as referred in, Scale bar=50 μm, $n = 3$. (D) H9c2 cells were analyzed by flow cytometry with DCFH-DA after 24-h treatment of DOX in combination with mitoTEMPO, PEG-SOD or KP. (E) Effect of mitoTEMPO, PEG-SOD or KP administration on DOX-induced oxidative stress damage markers SOD activity, $n = 3$. Data were expressed as mean ± SEM of three independent replicates; $^{###}P$ <0.001 vs. control group; $^{***}P$ < 0.001 vs. DOX group.

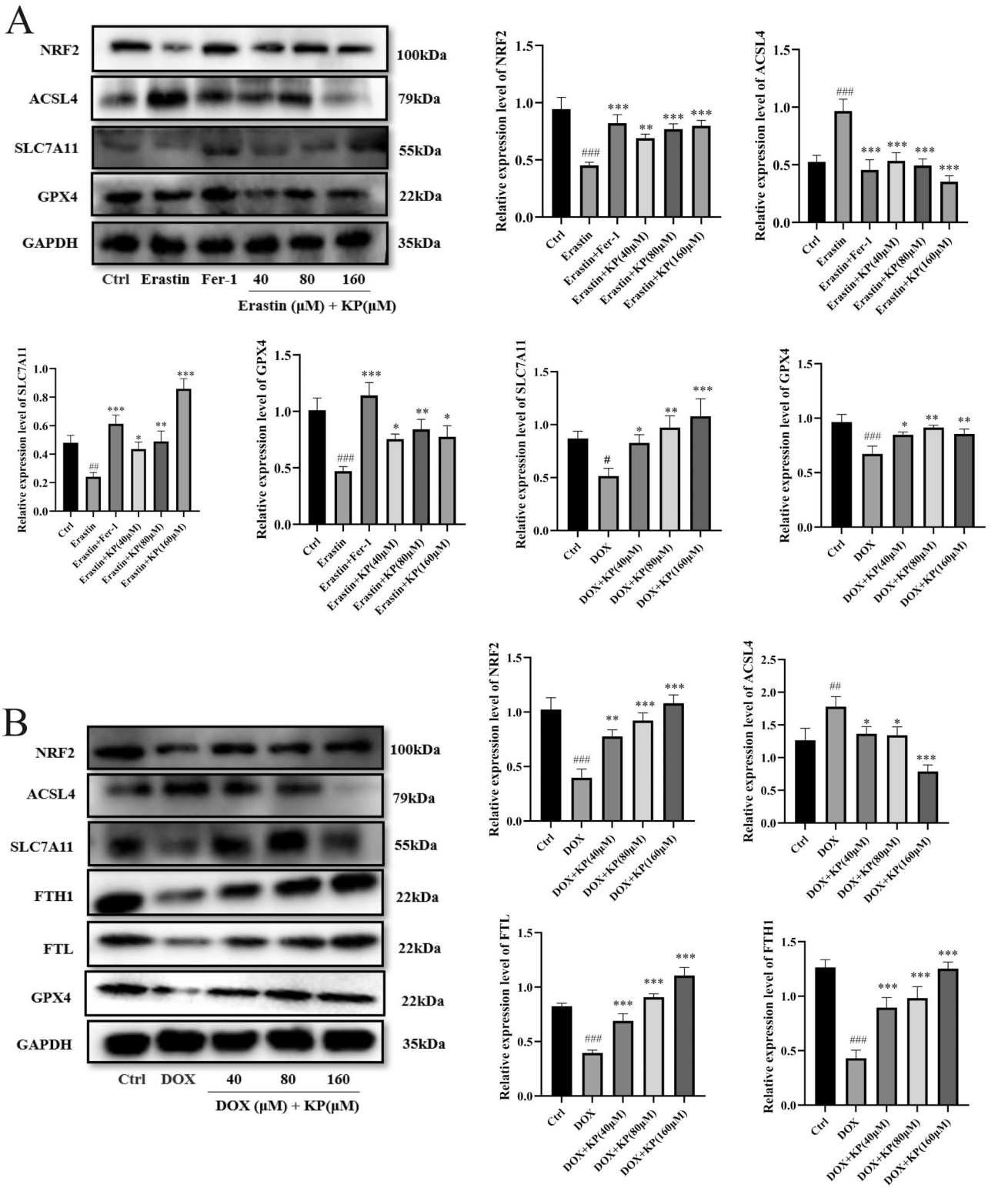

Figure 8. KP attenuated DOX cardiotoxicity by activating NRF2/SLC7A11/GPX4 pathway to suppress mitochondrial ROS-driven ferroptosis. (A,B) The expression levels of NRF2, ACSL4, SLC7A11 and GPX 4 in H9c2 cells with GAPDH as internal reference, $n = 3$. (B) The expression levels of NRF2, ACSL4, SLC7A11, FTL, FTH1 and GPX 4 in H9c2 cells with GAPDH as internal reference, $n = 3$. Data were expressed as mean ± SEM of three independent replicates; $^{\#}P < 0.05$, $^{\#\#}P < 0.01$, $^{\#\#\#}P < 0.001$ vs. control group; $^{*}P < 0.05$, $^{**}P < 0.01$, $^{***}P < 0.001$ vs. DOX group.

regulator NRF2 is involved in the defense against oxidative stress, which has been shown to regulate the expression of SLC7A11/GPX4 to inhibit ferroptosis [30]. Our experimental results showed KP's protective effects by restoring GSH levels and GPX4 activity, while downregulating the lipid peroxidation promoter ACSL4. The NRF2/SLC7A11/GPX4 pathway emerged as the linchpin of KP cardioprotection. KP promoted NRF2 nuclear translocation, transcriptionally activating SLC7A11 and GPX4 to enhance cystine uptake and GSH biosynthesis. This mechanistic cascade was validated by two complementary approaches: (1) The NRF2 activator TBHQ fully recapitulated KP effects on SLC7A11/GPX4 expression and mitochondrial function; (2) NRF2 siRNA abolished KP protective effects, confirming NRF2 indispensable role. These findings extend prior reports of NRF2 involvement in ferroptosis regulation [30] by delineating its mitochondrial-specific actions in cardiomyocytes. These results underscore KP ability to concurrently modulate iron

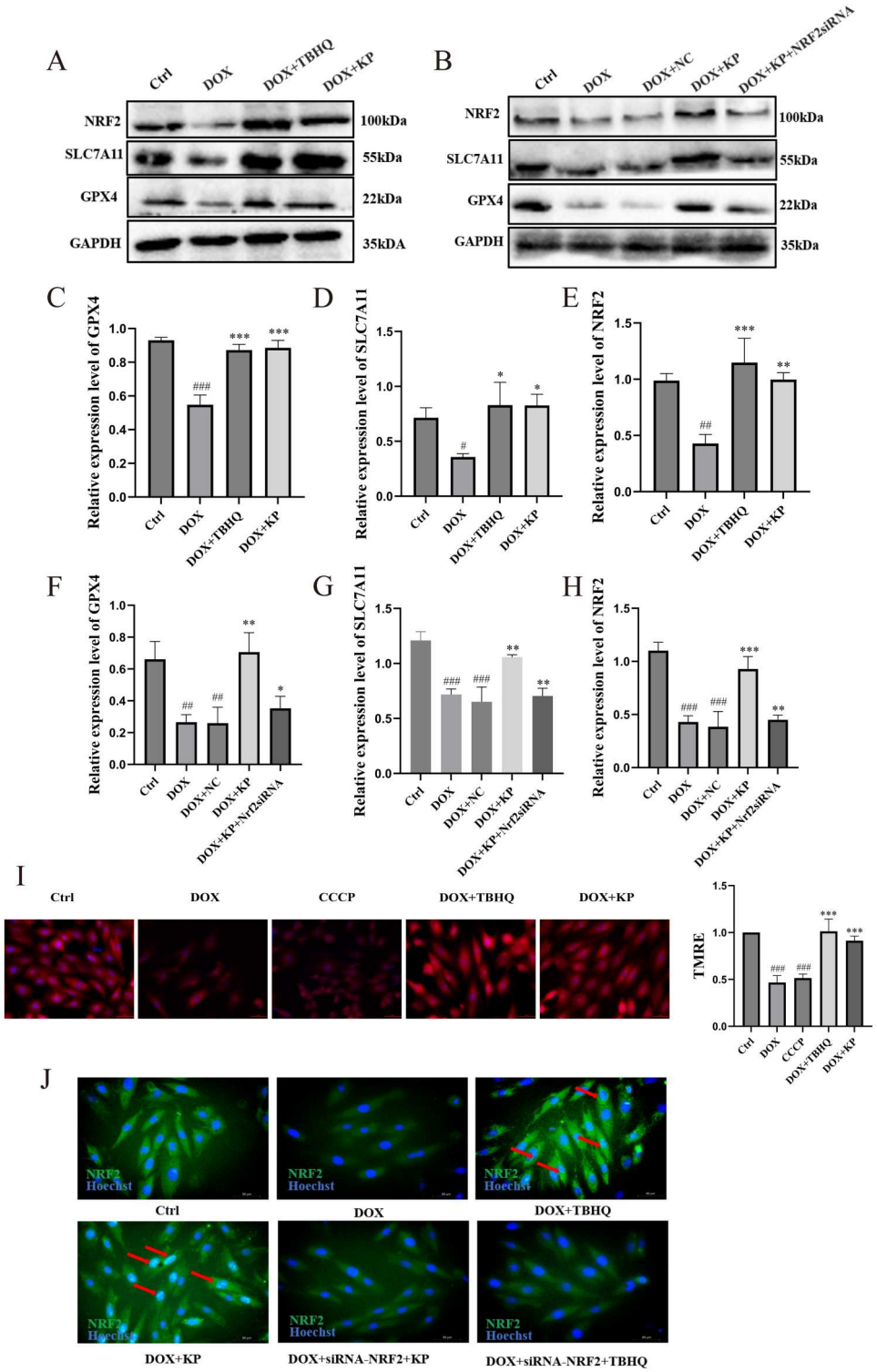

Figure 9. KP attenuated DOX cardiotoxicity by activating NRF2/SLC7A11/GPX4 pathway to suppress mitochondrial ROS-driven ferroptosis. (A–H) The expression levels of NRF2, SLC7A11 and GPX 4 in H9c2 cells with GAPDH as internal reference, $n = 3$. (I) Images of TMRE stained H9c2 cells after 24-h treatment of DOX in combination with or without TBHQ (2.5μM) or KP, Scale bar=50 μm, n=3. (J) Representative image of the effect of KP on NRF2 expression in DOX-stimulated cells. Scale bar = 50 μm, n=3. Data were expressed as mean ± SEM of three independent replicates; $^{\#}P < 0.05$, $^{\#\#}P < 0.01$, $^{\#\#\#}P < 0.001$ vs. control group; $^{*}P < 0.05$, $^{**}P < 0.01$, $^{***}P < 0.001$ vs. DOX group.

homeostasis and antioxidant defense through the NRF2/SLC7A11/GPX4 axis.

The cardiotoxic effects of DOX are driven by mitochondrial iron accumulation and subsequent ROS-dependent ferroptosis, as evidenced by DOX-induced mitochondrial Fe^{2+} accumulation and cristae disorganization. Mitochondria, as the primary site of DOX-induced lipid peroxidation [12], generate excessive ROS [31] that exacerbate oxidative stress and amplify ferroptosis [32]. To dissect the spatial regulation of ROS in ferroptosis, we employed two distinct superoxide scavengers: mitoTEMPO and PEG-SOD. Results showed that mitoTEMPO effectively suppressed mitochondrial ROS and lipid peroxidation, PEG-SOD reduced extracellular ROS, indicating that mitochondrial ROS are central to DOX cardiotoxicity. Notably, KP exhibited effects comparable to mitoTEMPO in restoring mitochondrial membrane potential and scavenging mitochondrial ROS. This suggests mechanism for KP: mitochondrial ROS clearance akin to mitoTEMPO. Compared

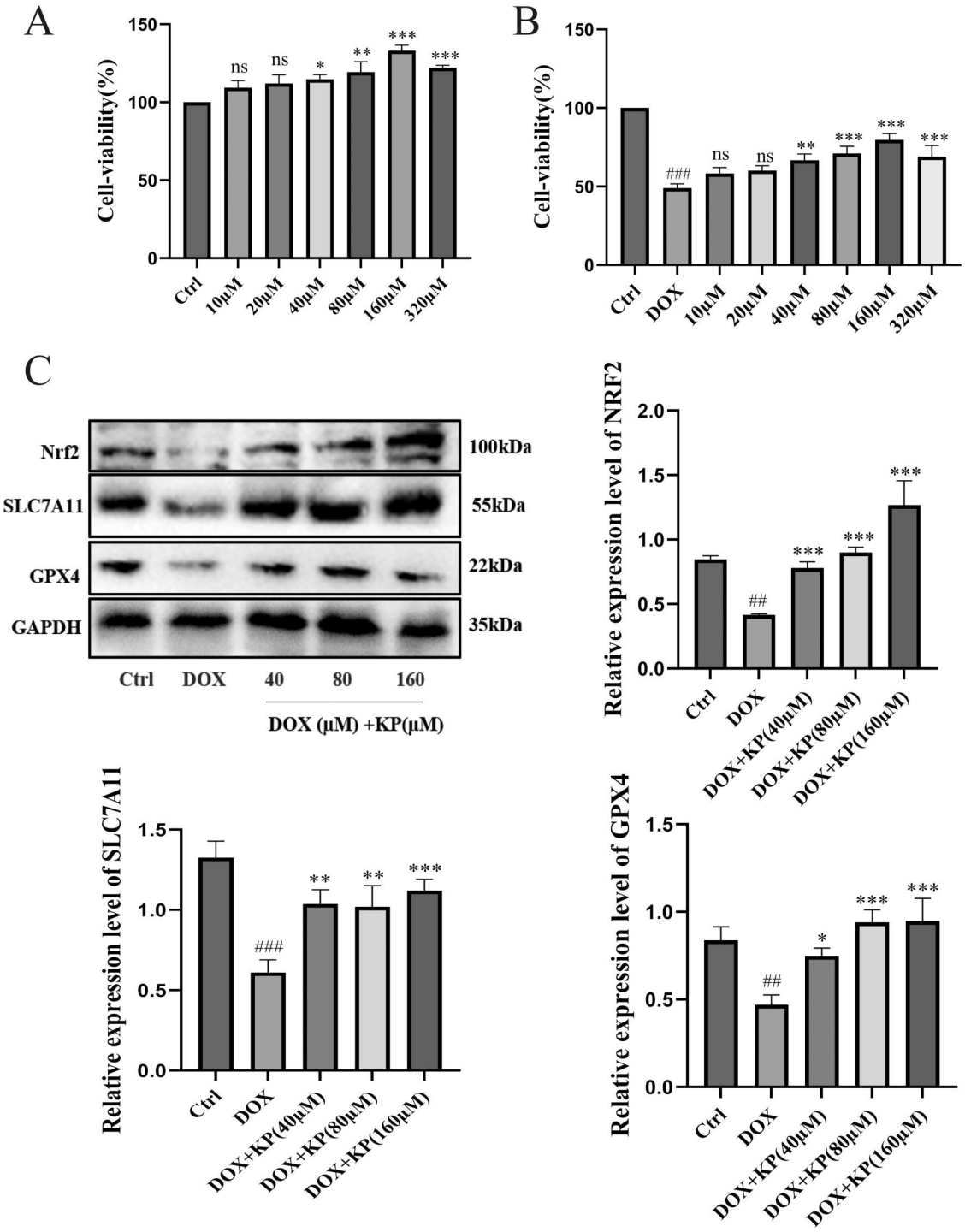

Figure 10. KP protected human AC16 cardiomyocytes from DOX-Induced ferroptosis via the NRF2/SLC7A11/GPX4 pathway (A) Cell viability assay of AC16 cardiomyocytes when treated with 0, 10, 20, 40, 80, 160, 320 μM of KP for 24-h, n=3. (B) AC16 cells were cultured with 2 μM DOX in combination with KP at various concentrations (0, 10, 20, 40, 80, 160, 320 μM) for 24-h. Cell viability was measured by MTT method, n=3. (C) The expression levels of NRF2, SLC7A11 and GPX 4 in H9c2 cells with GAPDH as internal reference, n=3. Data were expressed as mean ± SEM of three independent replicates; $^{\#\#}P < 0.01$, $^{\#\#\#}P < 0.001$ vs. control group; $^{*}P < 0.05$, $^{**}P < 0.01$, $^{***}P < 0.001$ vs. DOX group.

to multi-target agents like WGX50 [33] (mitochondrial ROS inhibition) and epigallocatechin-3-gallate [34] (AMPK/autophagy activation), KP ability to suppress ferroptosis in the integration of mitochondrial specificity and systemic antioxidant effects. While WGX50 focuses solely on mitochondrial ROS, KP additionally reversed DOX-induced SLC7A11/GPX4 downregulation and promoted NRF2 nuclear translocation, mechanisms critical for long-term antioxidant defense. Nevertheless, the exact contribution of extracellular SOD activation to KP effects remains unclear. Although KP reduced total ROS levels similarly to PEG-SOD, it is unknown whether this involves direct SOD enzymatic enhancement or indirect transcriptional regulation. Future studies should employ SOD activity assays and genetic knockdown models to delineate KP role in SOD modulation.

KP, a naturally occurring flavonoid abundant in various plants [13], exhibits diverse therapeutic properties, including antioxidant, anticancer, antiaging, and anti-inflammatory effects [15, 35–37]. Consuming of KP-rich vegetables and fruits may decrease the risk of certain cancers, including skin, liver, and colon [35]. To bridge translational gaps, we validated KP efficacy in human AC16 ventricular cardiomyocytes. KP rescued DOX-induced cell death and restored NRF2/SLC7A11/GPX4 pathway activity, demonstrating cross-

species conservation of its mechanism. This study first reveals KP inhibition of mitochondrial ROS-dependent ferroptosis against DOX-induced myocardial damage, though in vivo validation is essential; prior studies demonstrate KP efficacy in reversing pathological markers [37], mitigating mitochondrial damage, and restoring cardiac function in SD rat and chronic heart failure models [38], with cross-model consistency. *In vivo* metabolism studies reveal that KP is primarily converted into glucuronides, sulfates, and gut microbiota-derived phenolic acids [39, 40]. However, clinical translation of KP is hindered by low oral bioavailability and extensive first-pass metabolism. Metabolites like protocatechuic acid exert anti-inflammatory effects via localized deconjugation or NRF2 activation, whereas others such as 4-hydroxyphenylacetic acid remain functionally unclear due to insufficient systemic exposure [41–43]. To address these limitations, integrated strategies (including nanoparticle delivery systems, metabolomic profiling, and evaluation of bioactive derivatives) show promise in overcoming translational barriers. These innovations, combined with KP's robust in vitro efficacy and multi-target mechanisms, position it as a potential candidate for precision therapies, though further validation in advanced animal models remains critical.

5. Conclusion

This study demonstrates that KP alleviates DOX-induced myocardial injury by suppressing mitochondrial ROS-dependent ferroptosis. KP mitigates oxidative damage and ferroptosis through reducing mitochondrial iron overload, restoring mitochondrial membrane potential, and inhibiting ROS overproduction and lipid peroxidation. Mechanistically, KP activates the NRF2/SLC7A11/GPX4 axis, promoting NRF2 nuclear translocation and upregulating downstream antioxidant proteins to regulate iron homeostasis and lipid metabolism. While this study elucidates KP's mitochondrial-specific mechanisms, its efficacy in animal models and clinical translation requires further investigation. Future studies should explore KP's interactions with other cell death pathways and its potential in combination therapies for chemotherapy-induced cardiotoxicity.

Acknowledgements

We extend our gratitude to our colleagues for their invaluable efforts and insightful comments on this paper.

Author contributions

Lin Zhang: Conceptualization, Writing – review editing. Xiaorui Liu: Writing – original draft, preparation. Juan Wang: Data curation, Software. Zimu Li: Resources, Visualization. Siqi Wang: Methodology, Visualization: Wen Yang: Methodology, Validation. Yang Hai: Data curation. Dongling Liu: Supervision, Project administration.

Disclosure statement

No potential conflict of interest was reported by the author(s).

Funding

This project was supported by the National Natural Science Foundation of China [grant number 82074419], Gansu Provincial Science and Technology Plan Project [grant number 23JRRA1203 and 23JR6KA028] and Double First-Class Major Scientific Research Project of the Gansu Provincial Department of Education (GSSYLXM-05).

Data availability statement

All data from this study are available upon reasonable request by contacting the corresponding author.

References

[1] Volkova M, Russell R. Anthracycline cardiotoxicity: prevalence, pathogenesis and treatment. Curr Cardiol Rev. 2011;7(4):214–220. doi:10.2174/157340311799960645
[2] Groarke JD, Nohria A. Anthracycline cardiotoxicity: a new paradigm for an old classic. Circulation. 2015;131(22):1946–1949. doi:10.1161/circulationaha.115.016704
[3] Xu A, Deng F, Chen Y, et al. Nf-κB pathway activation during endothelial-to-mesenchymal transition in a rat model of doxorubicin-induced cardiotoxicity. Biomedicine & Pharmacotherapy = Biomedecine & Pharmacotherapie. 2020;130:110525. doi:10.1016/j.biopha.2020.110525
[4] Benjanuwattra J, Siri-Angkul N, Chattipakorn SC, et al. Doxorubicin and its proarrhythmic effects: A comprehensive review of the evidence from experimental and clinical studies. Pharmacol Res. 2020;151:104542. doi:10.1016/j.phrs.2019.104542
[5] Henriksen PA. Anthracycline cardiotoxicity: an update on mechanisms,: monitoring and prevention. Heart (British Cardiac Society). 2018;104(12):971–977. doi:10.1136/heartjnl-2017-312103
[6] Dixon SJ, Lemberg KM, Lamprecht MR, et al. Ferroptosis: an iron-dependent form of nonapoptotic cell death. Cell. 2012;149(5):1060–1072. doi:10.1016/j.cell.2012.03.042
[7] Chen X, Zeh HJ, Kang R, et al. Cell death in pancreatic cancer: from pathogenesis to therapy. Nat Rev Gastroenterol & Hepatol. 2021;18(11):804–823. doi:10.1038/s41575-021-00486-6
[8] Li N, Jiang W, Wang W, et al. Ferroptosis and its emerging roles in cardiovascular diseases. Pharmacol Res. 2021;166:105466. doi:10.1016/j.phrs.2021.105466
[9] Rabelo E, De Angelis K, Bock P, et al. Baroreflex sensitivity and oxidative stress in Adriamycin-induced heart failure. Hypertension (Dallas, Tex: 1979). 2001;38(3 Pt 2):576–580. doi:10.1161/hy09t1.096185
[10] Tadokoro T, Ikeda M, Ide T, et al. Mitochondria-dependent ferroptosis plays a pivotal role in doxorubicin cardiotoxicity. Jci Insight. 2020;5(9):1. doi:10.1172/jci.insight.132747
[11] Fang X, Wang H, Han D, et al. Ferroptosis as a target for protection against cardiomyopathy. Proc Natl Acad Sci U S A. 2019;116(7):2672–2680. doi:10.1073/pnas.1821022116
[12] Bai T, Li M, Liu Y, et al. Inhibition of ferroptosis alleviates atherosclerosis through attenuating lipid peroxidation and endothelial dysfunction in mouse aortic endothelial cell. Free Radical Biol Med. 2020;160:92–102. doi:10.1016/j.freeradbiomed.2020.07.026
[13] Wei Q, Jun L, Lei Z, et al. Kaempferol inhibits cisplatin-induced apoptosis in cardiomyocytes. Mol Cardiol China. 2017;17(01):1992–1995. doi:10.16563/j.cnki.1671-6272.2017.02.012
[14] Minotti G, Recalcati S, Menna P, et al. Doxorubicin cardiotoxicity and the control of iron metabolism: quinone-dependent and independent mechanisms. Methods Enzymol. 2004;378:340–361. doi:10.1016/s0076-6879(04)78025-8
[15] Xie F, Su M, Qiu W, et al. Kaempferol promotes apoptosis in human bladder cancer cells by inducing the tumor suppressor Pten. Int J Mol Sci. 2013;14(11):21215–21226. doi:10.3390/ijms141121215
[16] Guo Z, Liao Z, Huang L, et al. Kaempferol protects cardiomyocytes against anoxia/reoxygenation injury via mitochondrial pathway mediated by SIRT1. Eur J Pharmacol. 2015;761:245–253. doi:10.1016/j.ejphar.2015.05.056
[17] Wu W, Yang B, Qiao Y, et al. Kaempferol protects mitochondria and alleviates damages against endotheliotoxicity induced by doxorubicin. Biomed & Pharmacother Biomed & Pharmacother. 2020;126:110040. doi:10.1016/j.biopha.2020.110040
[18] Yuan Y, Zhai Y, Chen J, et al. Kaempferol ameliorates oxygen-glucose deprivation/reoxygenation-induced neuronal ferroptosis by activating Nrf2/SLC7A11/GPX4 axis. Biomolecules. 2021;11(7):923. doi:10.3390/biom11070923

[19] Li Q, Song Q, Pei H, et al. Emerging mechanisms of ferroptosis and its implications in lung cancer. Chin Med J (Engl). 2024;137(7):818–829. doi:10.1097/cm9.0000000000003048
[20] Vejpongsa P, Yeh ET. Topoisomerase 2β: a promising molecular target for primary prevention of anthracycline-induced cardiotoxicity. Clin Pharmacol Ther. 2014;95(1):45–52. doi:10.1038/clpt.2013.201
[21] Cardinale D, Colombo A, Bacchiani G, et al. Early detection of anthracycline cardiotoxicity and improvement with heart failure therapy. Circulation. 2015;131(22):1981–1988. doi:10.1161/circulationaha.114.013777
[22] Christidi E, Brunham LR. Regulated cell death pathways in doxorubicin-induced cardiotoxicity. Cell Death Dis. 2021;12(4):339. doi:10.1038/s41419-021-03614-x
[23] Wang K, Chen XZ, Wang YH, et al. Emerging roles of ferroptosis in cardiovascular diseases. Cell Death Discov. 2022;8(1):394. doi:10.1038/s41420-022-01183-2
[24] Stoyanovsky DA, Tyurina YY, Shrivastava I, et al. Iron catalysis of lipid peroxidation in ferroptosis: regulated enzymatic or random free radical reaction? Free Radical Biol Med. 2019;133:153–161. doi:10.1016/j.freeradbiomed.2018.09.008
[25] Zhou YJ, Duan DQ, Lu LQ, et al. The SPATA2/Cyld pathway contributes to doxorubicin-induced cardiomyocyte ferroptosis via enhancing ferritinophagy. Chem Biol Interact. 2022;368:110205. doi:10.1016/j.cbi.2022.110205
[26] Liu Y, Zeng L, Yang Y, et al. Acyl-CoA thioesterase 1 prevents cardiomyocytes from doxorubicin-induced ferroptosis via shaping the lipid composition. Cell Death Dis. 2020;11(9):756. doi:10.1038/s41419-020-02948-2
[27] Cao JY, Poddar A, Magtanong L, et al. A genome-wide haploid genetic screen identifies regulators of glutathione abundance and ferroptosis sensitivity. Cell Rep. 2019;26(6):1544–56.e8. doi:10.1016/j.celrep.2019.01.043
[28] Kang YP, Mockabee-Macias A, Jiang C, et al. Non-canonical glutamate-cysteine ligase activity protects against ferroptosis. Cell Metab. 2021;33(1):174–89.e7. doi:10.1016/j.cmet.2020.12.007
[29] Koppula P, Zhuang L, Gan B. Cystine transporter SLC7A11/xCT in cancer: ferroptosis,: nutrient dependency, and cancer therapy. Protein Cell. 2021;12(8):599–620. doi:10.1007/s13238-020-00789-5
[30] Wang X, Wang Y, Huang D, et al. Astragaloside Iv regulates the ferroptosis signaling pathway via the Nrf2/SLC7A11/GPX4 axis to inhibit PM2.5-mediated lung injury in mice. Int Immunopharmacol. 2022;112:109186. doi:10.1016/j.intimp.2022.109186
[31] Battaglia AM, Chirillo R, Aversa I, et al. Ferroptosis and cancer: mitochondria meet the "iron maiden" cell death. Cells. 2020;9(6):1505. doi:10.3390/cells9061505
[32] Stockwell BR. Ferroptosis turns 10: emerging mechanisms,: physiological functions, and therapeutic applications. Cell. 2022;185(14):2401–2421. doi:10.1016/j.cell.2022.06.003
[33] Tai P, Chen X, Jia G, et al. WGX50 mitigates doxorubicin-induced cardiotoxicity through inhibition of mitochondrial Ros and ferroptosis. J Transl Med. 2023;21(1):823. doi:10.1186/s12967-023-04715-1
[34] He H, Wang L, Qiao Y, et al. Epigallocatechin-3-gallate pretreatment alleviates doxorubicin-induced ferroptosis and cardiotoxicity by upregulating AMPKα2 and activating adaptive autophagy. Redox Biol. 2021;48:102185. doi:10.1016/j.redox.2021.102185
[35] Imran M, Salehi B, Sharifi-Rad J, et al. Kaempferol: A Key emphasis to Its anticancer potential. Molecules. 2019;24(12):2277. doi:10.3390/molecules24122277
[36] Suchal K, Malik S, Gamad N, et al. Kampeferol protects against oxidative stress and apoptotic damage in experimental model of isoproterenol-induced cardiac toxicity in rats. Phytomed: Int J Phytother Phytopharmacol. 2016;23(12):1401–1408. doi:10.1016/j.phymed.2016.07.015
[37] Xiao J, Sun GB, Sun B, et al. Kaempferol protects against doxorubicin-induced cardiotoxicity in vivo and in vitro. Toxicology. 2012;292(1):53–62. doi:10.1016/j.tox.2011.11.018
[38] Miaojuan Chen XL, Wang N. Effects and mechanisms of kaempferol on cardiac function in rats with chronic heart failure model. Adv Anat Sci. 2023 Jan;29(1):254-53.
[39] Berger A, Latimer S, Stutts LR, et al. Kaempferol as a precursor for ubiquinone (coenzyme Q) biosynthesis: an atypical node between specialized metabolism and primary metabolism. Curr Opin Plant Biol. 2022;66:102165. doi:10.1016/j.pbi.2021.102165
[40] Aa LX, Fei F, Qi Q, et al. Rebalancing of the gut flora and microbial metabolism is responsible for the anti-arthritis effect of kaempferol. Acta Pharmacol Sin. 2020;41(1):73–81. doi:10.1038/s41401-019-0279-8
[41] Bangar SP, Chaudhary V, Sharma N, et al. Kaempferol: a flavonoid with wider biological activities and its applications. Crit Rev Food Sci Nutr. 2023;63(28):9580–9604. doi:10.1080/10408398.2022.2067121
[42] Li S, Wang S, Zhang L, et al. Research progress on pharmacokinetics, anti-inflammatory and immunomodulatory effects of kaempferol. Int Immunopharmacol. 2025;152:114387. doi:10.1016/j.intimp.2025.114387
[43] Zabela V, Sampath C, Oufir M, et al. Pharmacokinetics of dietary kaempferol and its metabolite 4-hydroxyphenylacetic acid in rats. Fitoterapia. 2016;115:189–197. doi:10.1016/j.fitote.2016.10.008